Journal of
Manufacturing and Materials Processing

MDPI

Article

Design and Development of a Bespoke Rotary Friction Welding Machine in Exploration of Joining Dissimilar Materials for Nuclear Applications

Michail Dellepiane [1,*], Laurie Da Silva [2] and Athanasios Toumpis [1]

[1] Department of Mechanical & Aerospace Engineering, University of Strathclyde, Glasgow G1 1XJ, UK; athanasios.toumpis@strath.ac.uk
[2] Advanced Forming Research Centre (AFRC), University of Strathclyde, Renfrewshire PA4 9LJ, UK; laurie.da-silva@strath.ac.uk
* Correspondence: michail.dellepiane@strath.ac.uk

Abstract: Rotary friction welding is a solid-state welding process that can manufacture high-integrity joints between similar and dissimilar materials with short weld times. However, access to expensive and complex industrial-grade friction welding machines is not always possible. This study explores the design process and functionality of a laboratory-scale friction welding setup following the fundamentals of large-scale machinery. The proposed setup is designed to be easily manufactured, employing the use of a calibrated drill press and load cell, thus ensuring welding parameters such as rotational speed and applied axial load are monitored. The decision to investigate rotary friction welding of aluminium bronze Ca104 to austenitic stainless steel AISI316 was taken to explore the limitations of this bespoke friction welding machine for prospective applications in the nuclear energy sector. The workpieces were friction welded at four sets of rotational speeds with constant friction and forging pressures. The microstructural evolution and mechanical properties of the dissimilar material welds were investigated via optical and scanning electron microscopy with energy dispersive spectroscopy, 4-point bend testing and microhardness measurements. Results show a change in the hardness along the weld interface and evidence of metallic diffusion between the dissimilar materials, demonstrating the successful application of the small-scale experimental setup.

Keywords: dissimilar joining; rotary friction welding (RFW); lab-scale machinery; AISI316/Ca104 alloys; nuclear fusion applications; metallurgical investigation

Academic Editors: Xiaohong Lu, Daniel F.O. Braga and Sérgio Tavares

Received: 8 December 2024
Revised: 6 January 2025
Accepted: 7 January 2025
Published: 18 January 2025

Citation: Dellepiane, M.; Da Silva, L.; Toumpis, A. Design and Development of a Bespoke Rotary Friction Welding Machine in Exploration of Joining Dissimilar Materials for Nuclear Applications. *J. Manuf. Mater. Process.* **2025**, *9*, 27. https://doi.org/10.3390/jmmp9010027

1. Introduction

Joining of dissimilar materials has been a long-lasting endeavour for engineers due to the material's inherent differences in physical, mechanical, metallurgical, and thermal properties [1–3]. There has been an increased research interest for nuclear energy applications [4–7] of joined stainless steel and copper alloys. These sectors can greatly benefit from combining high strength, low thermal diffusivity, with high corrosion resistance, thermal and electrical conductivity. However, the materials' metallurgical incompatibility (solubility limits, solidification patterns, etc.) create challenges in their joining efforts [8]. Fusion-based welding processes present difficulties due to the varying properties of the materials involved [9,10]. Solid-state processes, however, maintain the integrity of the parent workpieces without requiring lower-grade filler metals usually found in fusion welding [11]. Rotary friction welding (RFW), a variant of friction welding, is a well-established solid

state joining process, proven capable of producing high-quality welds between workpieces of similar and dissimilar materials [12–14]. It is a technique frequently employing large industrial-scale machinery that is designed to convert mechanical energy into heat at the contact surfaces of the workpieces, with the help of an applied relative motion. Limited access to full-scale machinery restricts the range of research projects capable of utilising the fundamentals and advantages of friction welding. Thus, the need to investigate potential new outlets to design and develop small-scale, low-cost friction welding experimental setups with existing workshop machinery is created. This is further driven by the need to explore dissimilar materials compatibility for applications in demanding environments.

Across the available literature, researchers have been able to convert and utilise the functionality of a lathe for friction welding similar and dissimilar materials. Shah et al. [15] were able to design a fixture that would connect the pressure applying mechanism to the stationary workpiece, converting a conventional lathe machine into a low-cost friction welder. The experiments conducted expressed positive results for similar material friction welding such as stainless steel 070M20 and AA2011-T3 solid rounds of 10 mm and 12 mm diameters. Pressure was applied through a pneumatic system instead of a hydraulic one, often found in large-scale machinery. Rotational speed (rpm) was the main welding parameter with aluminium rods requiring much lower rpm compared to the welds conducted with the stainless steel rods. The most successful welds for the aluminium rods were identified at 1000 rpm, whereas for the stainless steel rods it was found to be 1400 rpm [15]. With rotational speed being directly proportional to the energy supplied to the system, welds at higher rpm led to increased temperatures generated at the weld interfaces, increasing the joint efficiency on the steel side. Arun et al. [16] successfully welded solid round rods of AA6063 with workpieces of 10 mm diameter by implementing a novel hydraulic hand pump that allowed the controlled application of axial pressure. Welding parameters such as friction pressure and time are predetermined with rotational speed and forging pressure being controlled over a range of experiments, with welds produced at 1000 rpm and 140 MPa, expressing the highest tensile strength at 210 MPa. Parandhaman et al. [17] explored the functionality of a conventional lathe without introducing any external components while using 12 mm diameter solid round rods of mild steel and AA6063. The provided results were limited, which further fortifies the need for this engineering task to be further explored and even consider other machinery such as a drill press.

Little exploration has been conducted on joining aluminium bronze (Ca104), a copper and iron alloy, to austenitic stainless steel (AISI316), in solid round geometries using a non-industry-scaled rotary friction welding setup. Tsuchiya et al. [18] investigated the optimum welding parameters that would be necessary to fabricate a joint between Cu-Cr-Zr/AISI316 metal alloys for magnetic fusion energy applications, such as high-heat flux components at the first wall of tokamak reactors, via friction welding. Welding parameters of 2200 rpm at 353 MPa and 608 MPa friction and forging pressures, respectively, with 9 s of total welding time exhibited tensile strength similar to the parent copper alloy. Optical microscopy showcased a narrow intermetallic compound (IMCs) layer between the faying surfaces of the workpieces, which was also the region of failure during tensile testing. The effect of friction welding parameters on the impact strength between copper and AISI430 was evaluated by Shanjeevi et al. [19]. Layers of IMCs that signify elemental segregation were found at the weld interfaces of every examined weld, which led to the degradation of their mechanical properties. A ductile mode of fracture with dimple formations was found at the interface of the fractured tensile samples in the thermomechanical affected zone (TMAZ) of the copper workpieces. In a follow-up study [20], the researchers examined the effect of welding parameters between AISI304L and oxygen-free copper. Across all

welded samples, the measured tensile strength never exceeded that of the copper parent material, with the ones performed at the highest rotational speed, 1500 rpm, being the closest. Overall results showed low percentages of joint efficiency between the dissimilar materials, with optical microscopy figures of the weld interface showing the stainless steel grains practically unaffected by the process, while copper had undergone drastic plastic deformation.

The primary engineering and scientific challenges in joining dissimilar materials, such as stainless steel and copper alloys, stem from their significant differences in physical, mechanical, and metallurgical properties. Metallurgical incompatibility, including solubility limits and the formation of intermetallic compounds (IMCs) at weld interfaces, often leads to mechanical property degradation and joint failure. The high-temperature sensitivity of these materials further complicates the control of welding parameters like rotational speed and friction pressure. Additionally, the lack of extensive research between those material combinations makes it challenging to optimise the process parameters for reliable, high-strength joints. While solid-state techniques such as rotary friction welding (RFW) show promise, access to large-scale machinery is limited, prompting the need for small-scale experimental setups. In this research paper, the effect of a range of rotational speeds was investigated on joining AISI 316 to aluminium bronze Ca104 solid round rods using a small-scale experimental friction welding setup. This study deepens the understanding of joining efforts between dissimilar metal alloys by generating welds and performing metallurgical and mechanical property investigations. A second key novelty showcased in this publication is the identification and development of a solution to this lack of access for large-scale machinery by implementing the fundamentals of friction welding with widely available laboratory equipment.

2. Materials and Methods

The solid round rods of the parent materials were machined to the following dimensions: 50 mm × 12 mm (length × diameter). The measured chemical composition of AISI316 and Ca104 are given in Tables 1 and 2, measured with a glow discharge optical emission spectrometer (GD-OES).

Table 1. Chemical composition of the AISI316 steel (weight %).

Fe	Cr	Ni	Mn	Mo	Si	C	Rest
67.55	16.83	11.15	1.51	2.1	0.365	0.023	0.472

Table 2. Chemical composition of aluminium bronze Ca104 alloy (weight %).

	Cu	Al	Fe	Ni	Mn
Min	83.5	8.50	4.00	4.00	-
Max	78	11.00	5.00	5.50	0.5

The employed welding process parameters are presented in Table 3. Loss of weld energy due to vibrations was prevented by having 2/3 of the total length of the workpieces secured inside the shaft of the friction welding machine. The applied axial load measurements using P = F/A (with area being the measured area of both workpieces before welding) was converted into friction and forging pressure, accordingly, as seen in Table 3. In total, 16 welds were produced, four for each set of parameters as per Table 3.

Table 3. Welding parameters applied during the RFW process.

Welds No.	RPM	Friction Pressure (MPa)	Forging Pressure (MPa)	Total Time (s)	Dwell Time (s)
1–4	800	18–28	8–14	25–35 s	5
5–8	1200	18–28	8–14	30–35 s	5
9–12	2200	18–28	8–14	20–25 s	5
13–16	3000	18–28	8–14	15–20 s	5

The manufactured joints of the dissimilar alloys were examined following the international standard BS EN ISO 15620 [21] used for friction welding metallic materials. Metallographic samples were machined and prepared following standard metallographic preparations and etched using a solution of 10% ferric nitride in distilled water. Optical and scanning electron microscopy were used to evaluate the microstructural evolution during the process as well as investigating any metallic diffusion via energy dispersive spectroscopy (EDS). The phase identification on the aluminium bronze alloy was further investigated via X-ray diffractometry (XRD). The welds were subjected to 4-point bend testing to determine flexural strength using the as-welded sample geometry. Vickers microhardness (HV) measurements were taken along the cross-sections of the welds in the form of line profiles in the center and outer regions, covering base material (BM), heat affected zone (HAZ), thermomechanically affected zone (TMAZ) and weld zone (WZ). A 0.5 HV load was applied over a 10 s dwell time and measurements were taken along the centre of the welds and along their outer area. The in-house assembly of the small-scale friction welding machine consisted of a load cell, workpiece housing shaft and support table with the addition of shoulder bolts. This assembly was designed with the rotating and fixed components safely secured during the welding process while allowing for ensuring accurate axial load applied readings. The full schematic and assembly can be seen in Figure 1.

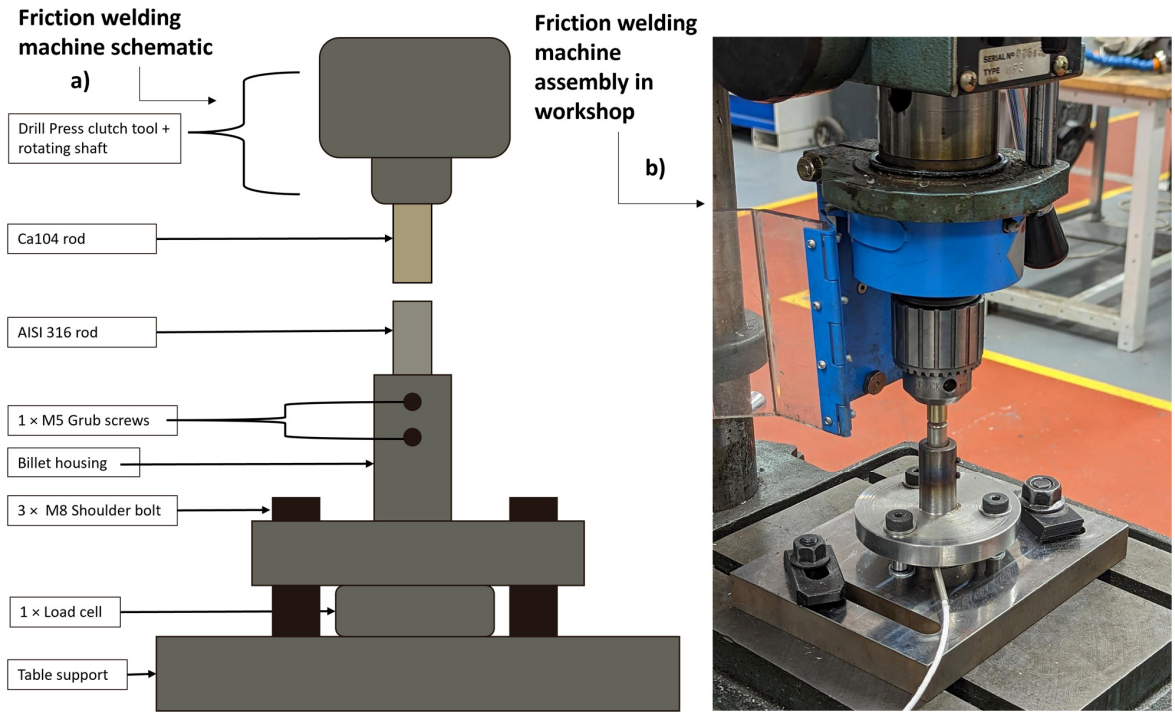

Figure 1. Small-scale friction welding machine schematic (**a**) + final assembly (**b**).

Workpiece stability during friction welding is of the highest importance to guarantee that the weld interface from both sides is in perfect alignment [22–24]. Pressure (frictional and forging) was applied manually compared to a large-scale, friction welding machine that employs a hydraulic pressure system. Additional machining was required on the non-rotating workpieces of the assembly so that both M5 grub screws hold the metal rods in place, replicating the jaws of a power drill chuck. A flat face of 35 mm × 5 mm (length × width) is machined to precise dimensions needed for this arrangement (Figure 2).

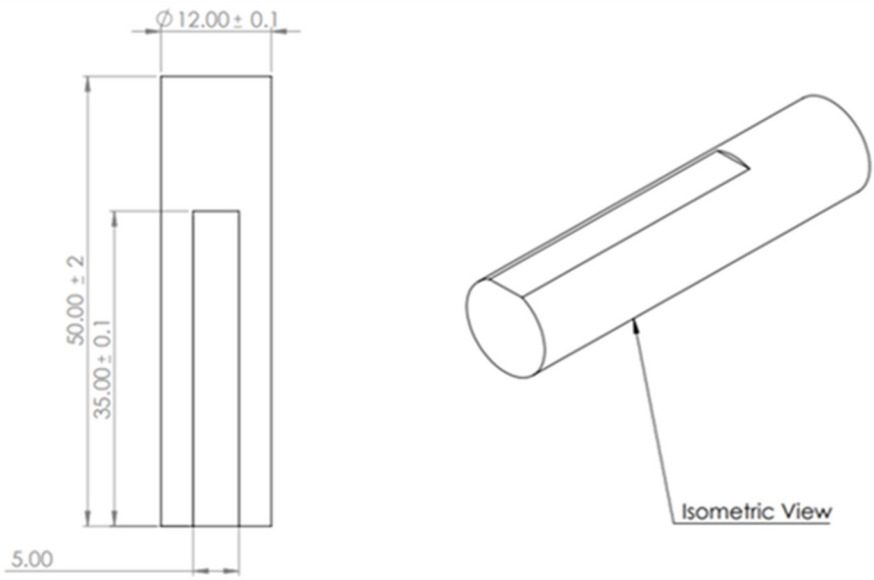

Figure 2. Fixed workpiece machining design (dimensions in mm).

3. Results and Discussion

Visual inspection of the stainless steel workpieces shows a discoloration near the contact area, with flash formed from the Ca104 side as seen in Figure 3. On average, the Ca104 rods experienced a total length reduction of approximately 7.3 mm from the initial 50 mm. There was no increase in upset and flash formation with the higher rotational speed joints.

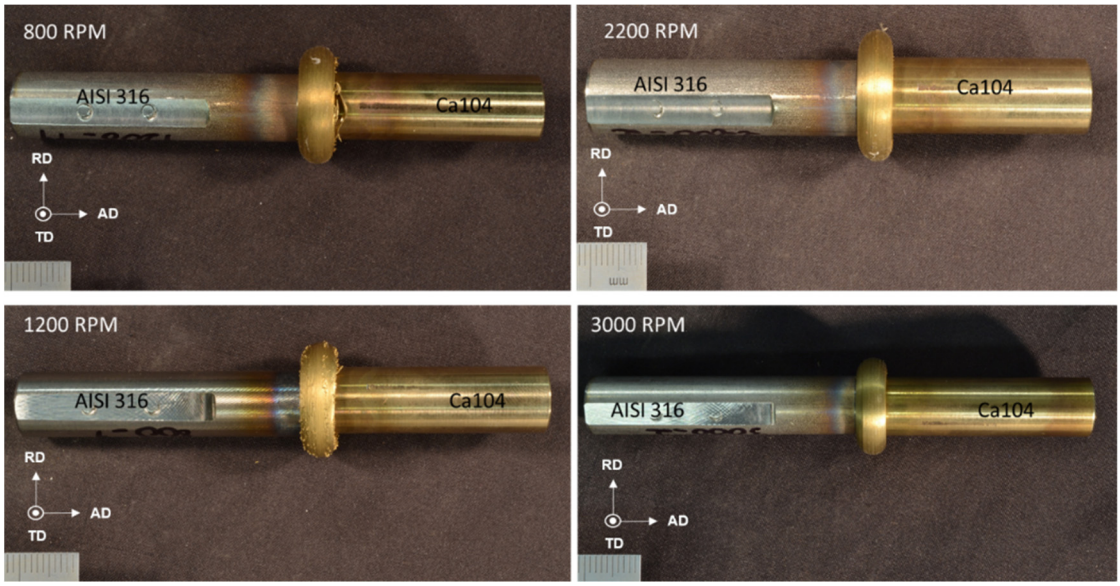

Figure 3. RFW joints of AISI316 to Ca104 utilising the capabilities of the small-scale friction welding machine. AD, TD and RD refer to the axial, radial and transverse directions, respectively.

3.1. Microstructural Characterisation

3.1.1. Optical Microscopy

The microstructure of the weld produced at 800 rpm is presented in Figure 4 in the axial direction (AD). The investigation is focused on the Ca104 side and not the AISI316 due to the former showcasing visible signs of deformation and change in microstructure. Grains in the BM exhibit linear directionality, seen in Figure 4a, and, as seen in Figure 4b,c, their elongated morphology has been transformed into fine spheroids towards the HAZ and TMAZ. The grain boundaries between TMAZ and WZ on Figure 4d are not as identifiable as in the BM (Figure 4a), due to the material becoming highly deformed, exhibiting martensitic structures as a result of fast cooling rates in the WZ towards the stainless steel side.

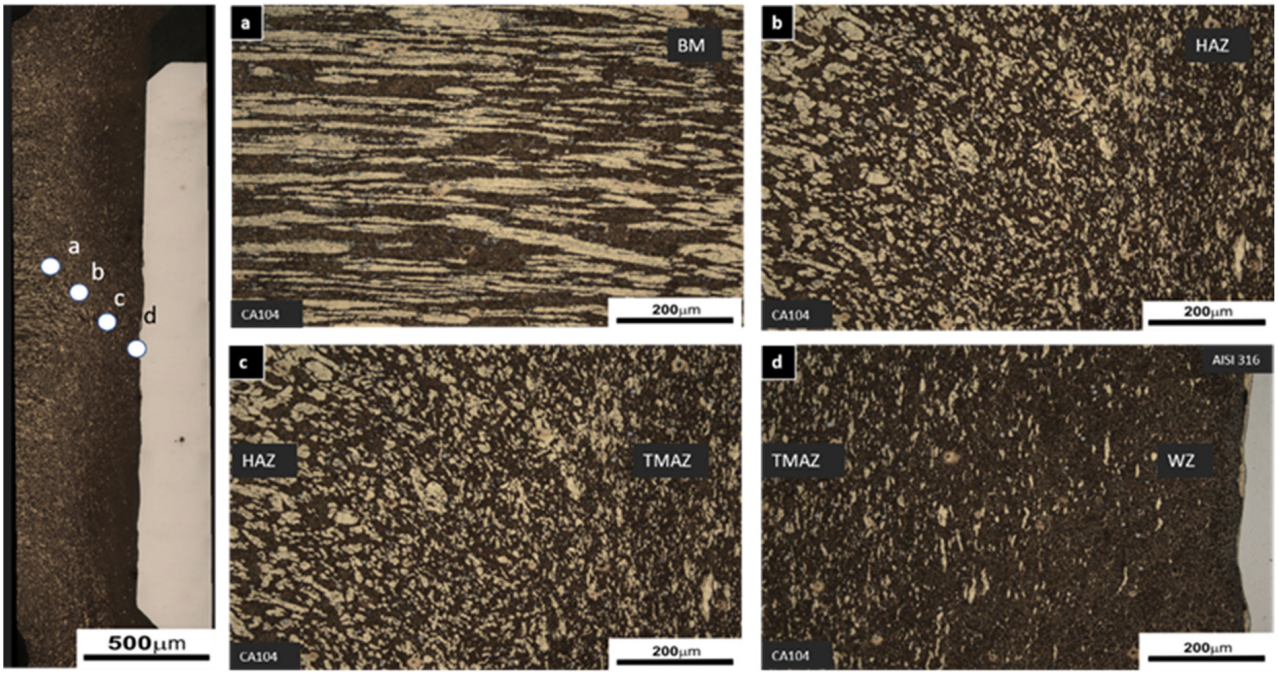

Figure 4. Microstructure of weld conducted at 800 rpm. BM, HAZ, TMAZ and WZ are provided accordingly (**a**–**d**).

The change of microstructure towards the weld interface at the WZ for welds performed at the higher rpm is equally important to consider on the Ca104 side, which is presented in Figure 5a–c (bright side is AISI316). Following the fundamentals of friction welding, when opting for higher rpm during the welding process, this equates to more energy supplied into the system [12]. A higher energy input during welding leads to higher temperatures between the workpieces at a much faster rate [25], allowing for a viscous flow and plastic deformation.

For the thermal energy to circulate along the axial direction, longer heated times are required, leading to a larger amount of material heated. According to Banerjee et al. [26], the amount of heat dissipated or transferred to the adjustment regimes is directly proportional to the weld energy and is expressed as:

$$Q = \frac{\pi^2 P \mu N R^3}{20} \quad (1)$$

where Q, P, R, N and μ represent the heat, pressure, radius of the weld component, rotational speed and coefficient of friction, respectively. A challenge when exploring friction welding of dissimilar materials is reducing the formation of intermetallic compounds at the joint interfaces, which are brittle and negatively affect the mechanical properties of the weld [27].

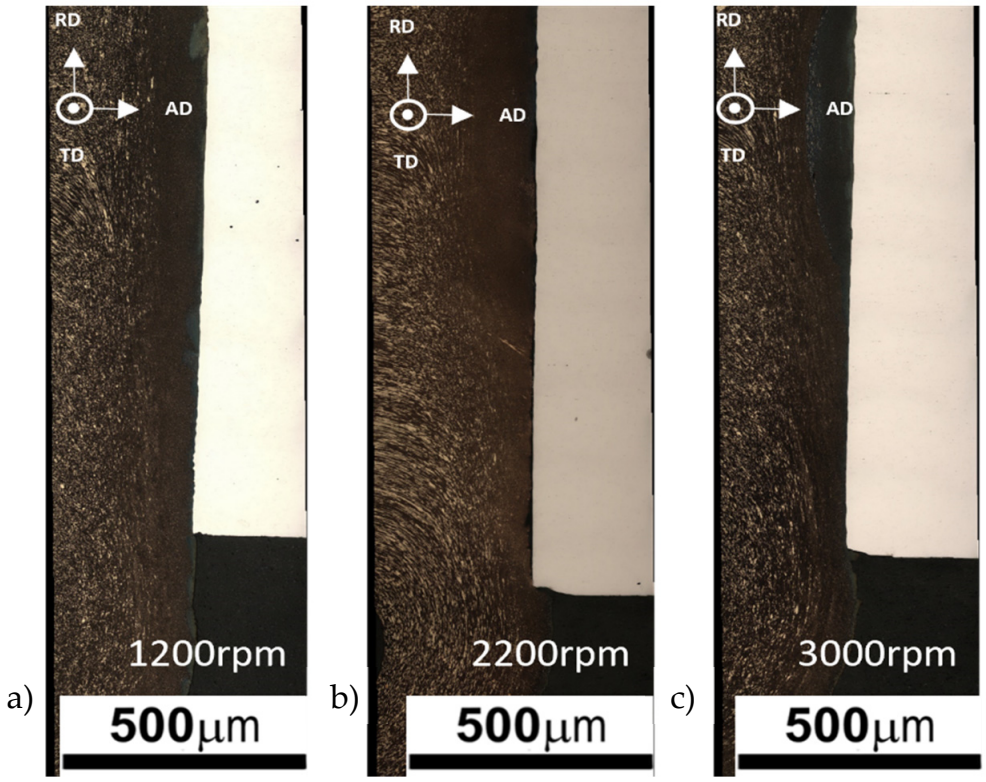

Figure 5. Microstructure of welds conducted at 1200, 2200 and 3000 rpm, respectively (**a**–**c**). AD, TD and RD refer to the axial, radial and transverse directions, respectively

3.1.2. Phase Identification of Ca104

Stainless steel is an alloy of Fe-Cr-Ni (with additions of Mn, Mo, Si and C) and has a face-centred cubic (FCC) crystal structure which is the product of the addition of Ni to the Fe, eliminating the ductile-to-brittle transitional behaviour of Fe [8,28]. Oxygen free copper is a metal with an inherent FCC crystal structure; however, with the inclusion of Fe, Ni and Mn in the Ca104, it is also considered a copper alloy with additional phases within the crystal structure [29–31].

XRD analysis was employed to determine the space groups of the identified crystal structures on the aluminium bronze side, which are provided in Figure 6. This analysis has helped identify the current phases found in both the BM and WZ as shown in Figure 7a,b. Within the three-dimensional micellar sphere packing, there are three identified space groups that are correlated to a specific crystal structure [32]. Im-3m is a BCC structure, Fm-3m is FCC and $P6_3/mmc$ is HCP. The space groups identified on the Ca104 workpiece are two, Im-3m and Fm-3m, indicating the existence of both α phase with an FCC and β phase with a BCC crystal structure, as reported by Xu et al. [33]. The existence of these phases can significantly alter the corrosion resistance of the aluminium bronze alloy [29,34]. In addition to the existing phases, metastable intermetallic k particles are present, scattered throughout the microstructure of Ca104, which are directly correlated to the dynamic softening of the material that is recorded [33]. The existing phases in the crystal matrix and the additional particles are identified in Figure 7.

3.1.3. Elemental Diffusion Investigation

Elemental diffusion can be considered to be a complimentary bonding mechanism in friction welding of metallic systems [11,35–37] and the evidence of it can demonstrate a higher-quality weld [11,37,38]. SEM images and the location of the line scan analysis performed at the weld interfaces of the AISI316 to Ca104 rotary friction welds are provided

in Figure 8. Each data point of the scanned lines has been plotted in Figure 9, for each element identified in both materials, as described in Tables 1 and 2. The penetration of Cr and Fe, respectively, is measured to a depth of 0.5–2.3 μm from the AISI316 side to the Ca104 side. In contrast, no traces of Cu or Al can be found on the AISI316 side, signifying that the temperatures generated at the interface were not high enough to create diffusion conditions for the stainless steel side. This can be linked to the limitations of the suggested friction welding setup. Studies have presented indicative temperatures where Cu has been found to diffuse into stainless steel as high as 950 °C [36,39], while Cr can diffuse into Fe-Cr systems as low as 600 °C [40–42]. Out of all the welds investigated, the one produced at 3000 rpm showcased the deepest penetration of Cr and Fe from the AISI316 to the Ca104 side at a depth of 2.2 μm. This can be linked to the fact that the higher rotational speed on the interface is directly correlated to a higher heat input between the workpieces, suggesting higher temperatures generated while welding. The opposite is found for the weld at 800 rpm, where the Cr diffusion can be found at depths of 0.5 μm, i.e., a decrease of 77.72%.

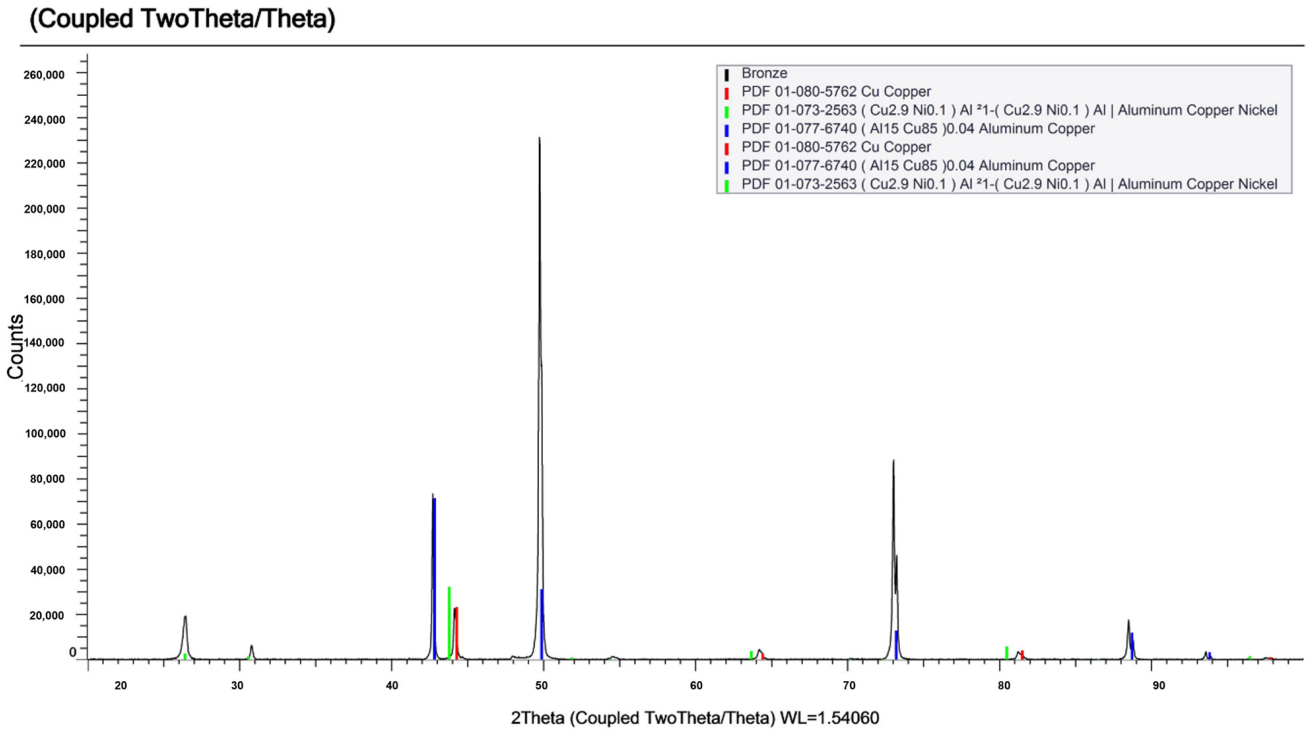

Formula	Quality	Y-Scale	I/Ic DB	I/Ic User	S-Q	Concentration Level	d x by
Cu	Hypothetical	9.48 %	12.070	0.000	13.9 %	Major	1.0000
(Cu2.9 Ni0.1) Al	Indexed	13.16 %	10.430	0.000	22.4 %	Major	1.0000
(Al15 Cu85)0.04	Indexed	29.32 %	8.160	0.000	63.7 %	Major	1.0000

Scan WL	System	Space Group	a	b	c	alpha	beta	gamma	Z	Volume
Yes	Cubic	Im-3m (229)	2.89000 Å						2	24.14 Å³
Yes	Cubic	Fm-3m (225)	5.84120 Å						4	199.30 Å³
Yes	Cubic	Fm-3m (225)	3.65360 Å						1	48.77 Å³

Figure 6. XRD analysis results of Ca104.

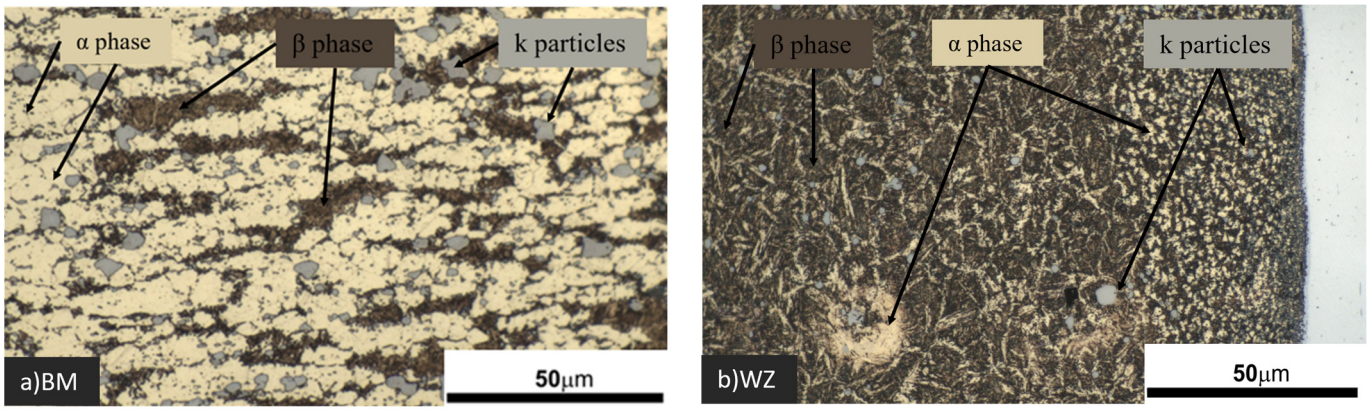

Figure 7. Micromorphology of aluminium bronze in the BM (**a**) and WZ (**b**).

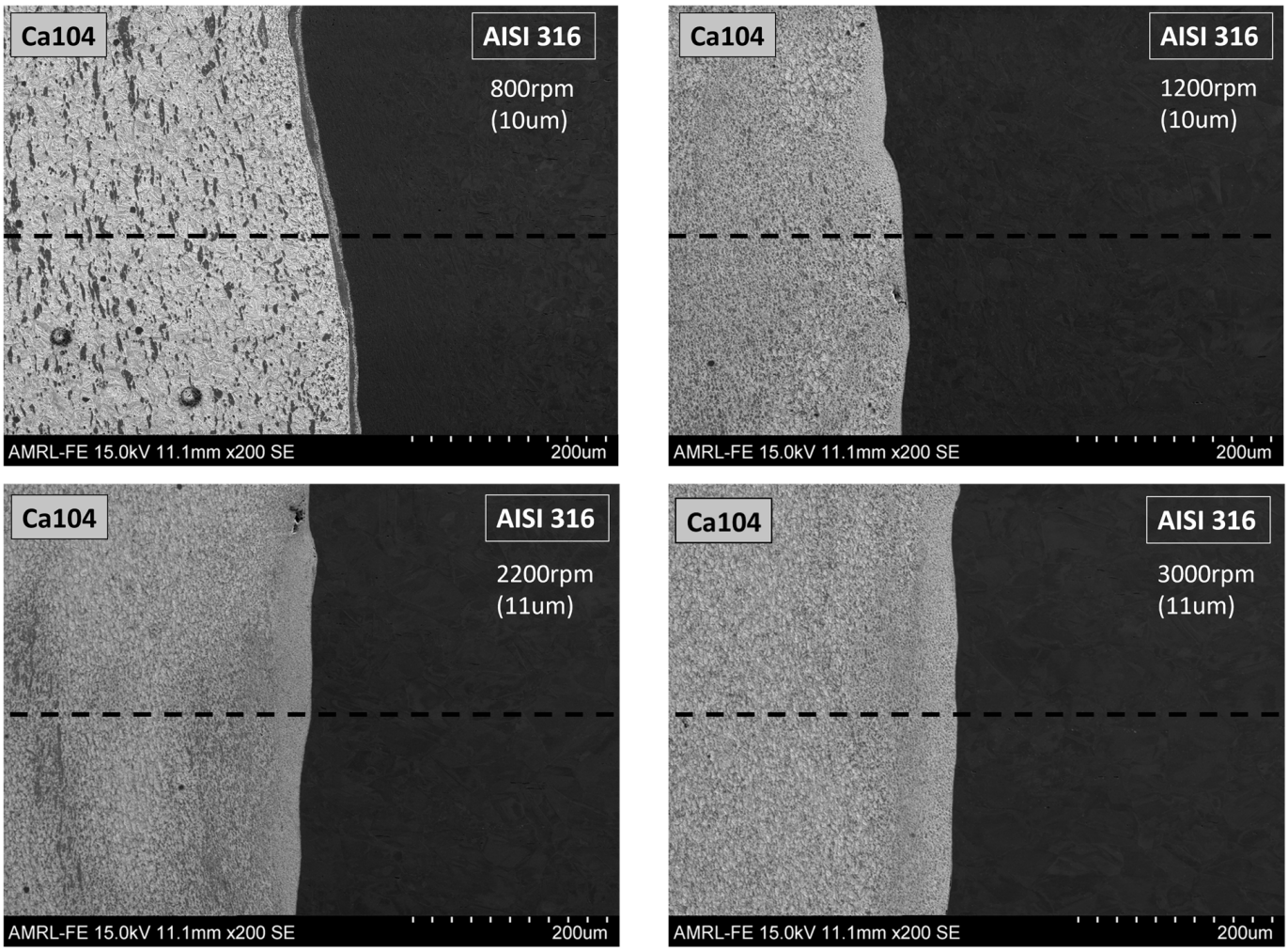

Figure 8. SEM micrographs of the friction welds at the interface where the EDS line analysis was taken: 800 rpm, 1200 rpm, 2200 rpm and 3000 rpm, respectively.

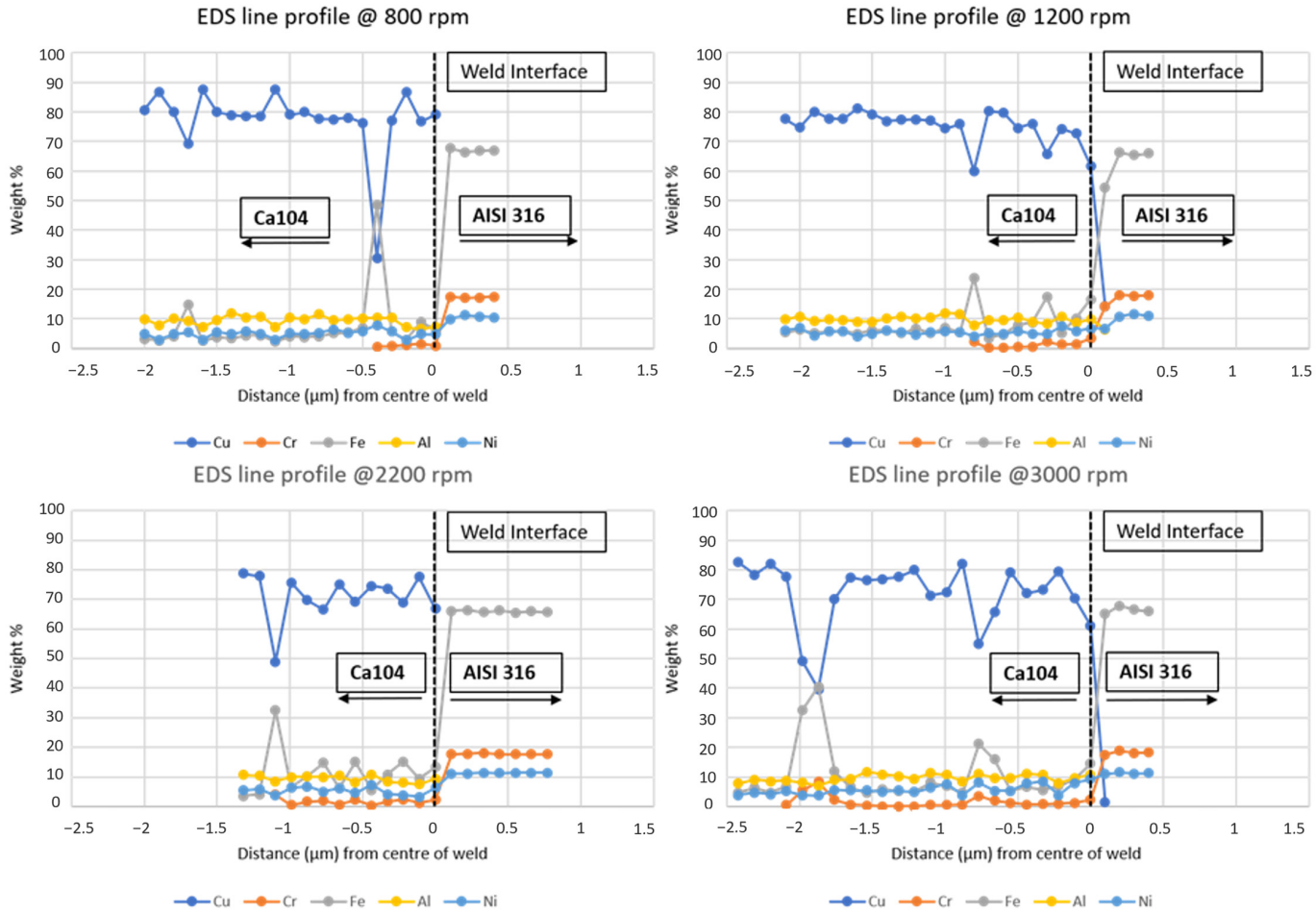

Figure 9. Elemental distribution at the centre of the welds showcasing diffusion of chromium and iron from AISI316 to the Ca104 for each weld: 800 rpm, 1200 rpm, 2200 rpm and 3000 rpm, respectively.

3.2. Mechanical Properties

3.2.1. Flexural Strength Analysis

The flexural strength of the dissimilar material welds was examined by subjecting samples to a 4-point bend testing regime. The flexural strength of each weld was measured, and their average value was compared to that of the BM, as seen in Figure 10. The 4-point bend test results were examined in sets of three samples per set of welding parameters. For every set of parameters, all samples failed at the weld interface of both workpieces with relative homogeneity, as seen in Figure 11 at 800 rpm, while displaying a higher flexural strength than that of AISI316 with a mean value of 258 MPa. The samples showcase uniform brittle failure with micro-traces of Ca104 on the AISI316 workpieces. Amongst the four examined sets, the welds joined at 1200 rpm exhibited the highest average flexural strength of 386 MPa, while the welds joined at 2200 rpm had the lowest average flexural strength of 308 MPa. Ductility measurements taken from all examined welds showcased no additional increase for that of the base materials. Contrary to maximum diffusion correlation with highest rpm, maximum bond strength does not occur at highest rpm due to the other material interdependencies. This is again supported by the statement that diffusion bonding is an aspect of complete metallurgical bonding between dissimilar alloys [43,44].

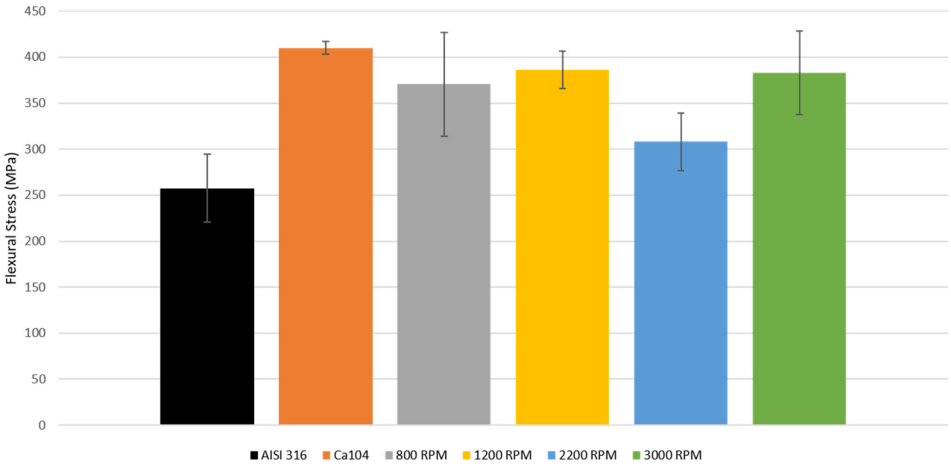

Figure 10. Flexural strength comparison of parent materials vs rotary friction welds at variable rotational speeds with standard error bars.

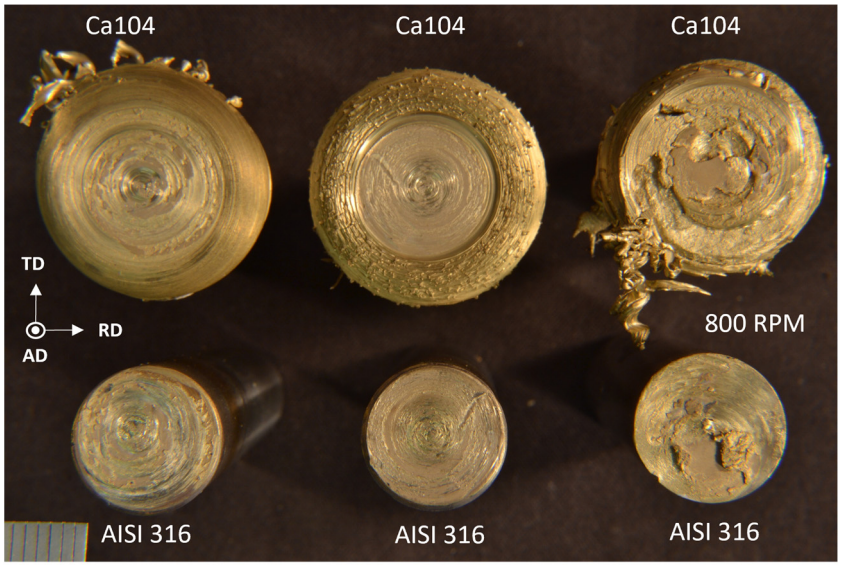

Figure 11. Fractured 4-point bend testing RFW joints of AISI316 to Ca104 at 800 rpm. AD, TD and RD refer to the axial, radial and transverse directions, respectively.

3.2.2. Hardness Distribution

The hardness distribution of AISI 316 to Ca104 rotary friction welds for each set of parameters is represented in Figure 12 for the outer region and centre region along the axis of the welded joint. The hardness values of the parent materials are measured within the range of 190–220 HV for AISI316 and 195–210 HV for Ca104. Both graphs follow a similar trend of hardness evolution with the only difference found in the outer region (Figure 12a), where all four welds experienced a steeper increase from the HAZ to TMAZ on the Ca104 side. The finer-grained microstructure that is found in the TMAZ and WZ of the Ca104 was responsible for the highest hardness values. This hardness increase can be attributed to the grain refinement experienced by the material as a result of dynamic recrystallisation which has been reported in similar studies [45–47], further supported by the microstructure changes presented in Figure 4. Furthermore, there is a decreasing trend from the weld's centre towards the parent material, with a steep transition between the WZ, TMAZ and HAZ. The maximum hardness in the WZ from the Ca104 side was measured at 268, 255, 277 and 270 for 800, 1200, 2200 and 3000 rpm, respectively, indicating minor changes in hardness with increasing rotational speed. Nevertheless, a decrease in rotational speed led

to a lower generation of heat that may result in a smaller fraction of grain refinement and conservation of the original microstructure in the WZ post-cooling (i.e., higher ductility, decreased hardness).

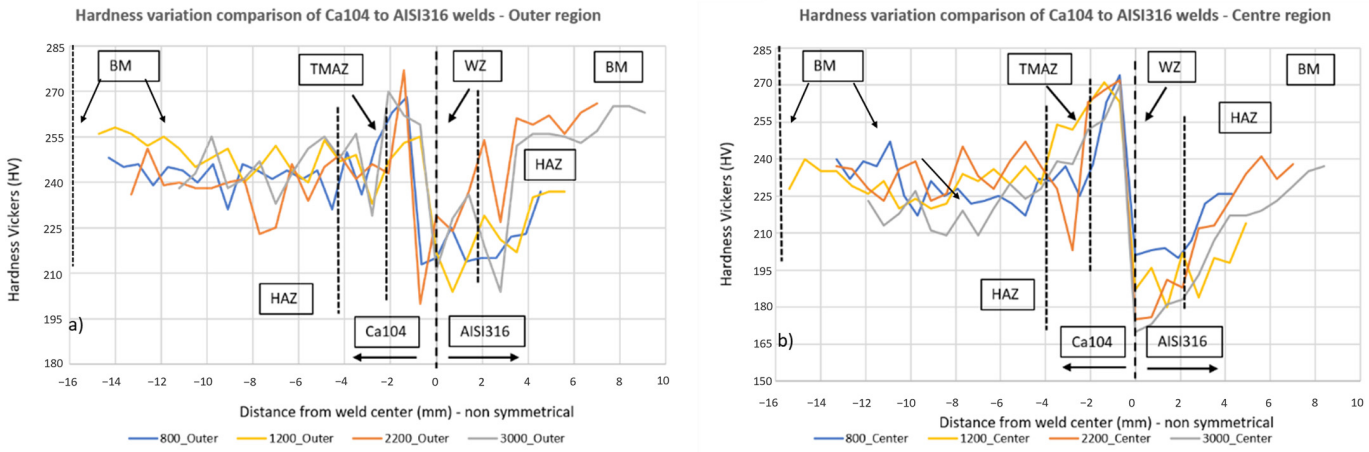

Figure 12. Microhardness evolution along the length of the welded samples for all 4 rotational speeds in the outer and centre region, (**a**,**b**).

4. Conclusions

In this present study, the capabilities of a bespoke laboratory-scale, rotary friction welding machine were explored. Solid cylindrical rods of AISI316 and Ca104 were rotary friction welded with four sets of welding parameters and subject to metallographic and mechanical property investigations to assess the joint integrity. The key findings of this study are summarised as the following:

1. Based on the principles of already existing industry-grade friction welding machines, it was made possible to design and manufacture components that, when used in conjunction with a drill press, allowed for the exploration of friction of welding dissimilar metals. Friction welding of dissimilar materials was made possible employing this experimental, small-scale friction welding machine.
2. Changes in the microstructure of the Ca104 alloy were visible with grains transforming from an elongated to a fine equiaxed shape near the weld interface with the material becoming heavily deformed. This is envisaged to be due to the fact that the grains have experienced dynamic recrystallisation during welding.
3. The existence of two different crystal structures and the presence of intermetallic k particles on the Ca104 is demonstrated through XRD analysis.
4. EDS analysis showed that Cr diffused further from the AISI316 side to Ca104 when increasing rotational speed as a result of the higher heat input. However, temperatures at the weld interface were not high enough to promote Cu diffusion into the AISI316 workpiece. The greater the difference in concentration, the quicker will be the rate of diffusion between the dissimilar metals.
5. All four sets of weld parameters generated joints between the dissimilar materials with a flexural strength higher than that of the AISI316 base material.
6. The microhardness evolution in two different regions for each weld showed a similar trend of increase and decrease, with the hardness in the WZ of the Ca104 being the highest at 268, 255, 277 and 270 HV for 800, 1200, 2200 and 3000 rpm, respectively.

Author Contributions: Conceptualization, M.D.; methodology, M.D.; formal analysis, M.D.; investigation, M.D.; resources, M.D.; data curation, M.D.; writing—original draft preparation, M.D.; writing—review and editing, M.D., L.D.S. and A.T.; visualization, M.D.; supervision, A.T. and L.D.S.;

project administration, M.D.; funding acquisition, L.D.S. and A.T. All authors have read and agreed to the published version of the manuscript.

Funding: This research received no external funding.

Data Availability Statement: Data are contained within the article.

Conflicts of Interest: The authors declare no conflicts of interest.

References

1. Satyanarayana, V.V.; Madhusudhan Reddy, G.; Mohandas, T. Dissimilar metal friction welding of austenitic–ferritic stainless steels. *J. Mater. Process. Technol.* **2005**, *160*, 128–137. [CrossRef]
2. Sahin, M. Joining of stainless steel and copper materials with friction welding. *Ind. Lubr. Tribol.* **2009**, *61*, 319–324. [CrossRef]
3. Kim, S.-Y.; Jung, S.-B.; Shur, C.-C.; Yeon, Y.-M.; Kim, D.-U. Mechanical properties of copper to titanium joined by friction welding. *J. Mater. Sci.* **2003**, *38*, 1281–1287. [CrossRef]
4. Dai, Y.; Zheng, X.; Ding, P. Review on sodium corrosion evolution of nuclear-grade 316 stainless steel for sodium-cooled fast reactor applications. *Nucl. Eng. Technol.* **2021**, *53*, 3474–3490. [CrossRef]
5. Maziasz, P.; Busby, J.T. Properties of Austenitic Steels for Nuclear Reactor Applications. *Compr. Nucl. Mater.* **2012**, *2*, 267–283. [CrossRef]
6. Harling, O.K.; Yu, G.P.; Grant, N.J.; Meyer, J.E. Application of high strength copper alloys for a fusion reactor first wall. *J. Nucl. Mater.* **1981**, *103*, 127–132. [CrossRef]
7. Fabritsiev, S.A.; Zinkle, S.J.; Singh, B.N. Evaluation of copper alloys for fusion reactor divertor and first wall components. *J. Nucl. Mater.* **1996**, *233–237*, 127–137. [CrossRef]
8. Joshi, G.R.; Badheka, V.J.; Darji, R.S.; Oza, A.D.; Pathak, V.J.; Burduhos-Nergis, D.D.; Burduhos-Nergis, D.P.; Narwade, G.; Thirunavukarasu, G. The Joining of Copper to Stainless Steel by Solid-State Welding Processes: A Review. *Materials* **2022**, *15*, 7234. [CrossRef]
9. Baeslack, W.A., III; Duquette, D.J.; Savage, W.F. The Effect of Ferrite Content on Stress Corrosion Cracking in Duplex Stainless Steel Weld Metals at Room Temperature. *Corrosion* **2013**, *35*, 45–54. [CrossRef]
10. Jannet, S. Comparative investigation of friction stir welding and fusion welding of 6061 T6—5083 O aluminum alloy based on mechanical properties and microstructure. *Bull. Pol. Acad. Sci. Tech. Sci.* **2014**, *62*. [CrossRef]
11. Khedr, M.; Hamada, A.; Järvenpää, A.; Elkatatny, S.; Abd-Elaziem, W. Review on the Solid-State Welding of Steels: Diffusion Bonding and Friction Stir Welding Processes. *Metals* **2023**, *13*, 54. [CrossRef]
12. Maalekian, M.; Kozeschnik, E.; Brantner, H.P.; Cerjak, H. Comparative analysis of heat generation in friction welding of steel bars. *Acta Mater.* **2008**, *56*, 2843–2855. [CrossRef]
13. Maalekian, M. Friction welding—Critical assessment of literature. *Sci. Technol. Weld. Join.* **2007**, *12*, 738–759. [CrossRef]
14. Jayabharath, K.; Ashfaq, M.; Venugopal, P.; Achar, D.R.G. Investigations on the continuous drive friction welding of sintered powder metallurgical (P/M) steel and wrought copper parts. *Mater. Sci. Eng. A* **2007**, *454–455*, 114–123. [CrossRef]
15. Shah, K.; Khurshid, H.; Haq, I.; Khurram, N.; Ali, Z. Conversion of a Conventional Lathe Machine into a Friction Welding Machine and Performing Some Experimental Tests for its Operational Feasibility. *Mehran Univ. Res. J. Eng. Technol.* **2021**, *40*, 545–555. [CrossRef]
16. Arun, P.B.; Yadhu, V.; Sanalkumar, C.S. To Design and Construct a Friction Welding Attachment on Lathe, Conduct Experiment and to Study about Mechanical Behavior of Friction Welded Joints of Aluminum Rods. *Int. J. Eng. Res.* **2017**, *V6*, 150–158. [CrossRef]
17. Bparandhaman, M.E.; Prema, M.; Indhumathi, E.; Nivedha, M.; Thamizharasi, D. Analysis of friction welding in conventional lathe machine. *Int. J. Pure Appl. Math.* **2018**, *119*, 14549–14554.
18. Tsuchiya, K.; Kawamura, H. Mechanical properties of CuCrZr alloy and SS316 joints fabricated by friction welding method. *J. Nucl. Mater.* **1996**, *233–237*, 913–917. [CrossRef]
19. Shanjeevi, C.; Arputhabalan, J.J.; Dutta, R. Investigation on the Effect of Friction Welding Parameters on Impact Strength in Dissimilar Joints. *IOP Conf. Ser. Mater. Sci. Eng.* **2017**, *197*, 012069. [CrossRef]
20. Chinnakannan, S. Friction Welding of Austenitic Stainless Steel with Copper Material. *Austenitic Stainl. Steels-New Asp.* **2017**, 171–186. [CrossRef]
21. *Din En ISO 15620:2019*; Friction Welding of Metallic Materials. International Organization for Standardization: Geneva, Switzerland, 2019; pp. 1–5.
22. Dilthey, U. Joining of Metals. In *Encyclopedia of Materials Science and Technology*; Buschow, K.H.J., Cahn, R.W., Flemings, M.C., Ilschner, B., Kramer, E.J., Mahajan, S., Veyssière, P., Eds.; Elsevier: Oxford, UK, 2001; pp. 4338–4341. [CrossRef]

23. Schmicker, D.; Naumenko, K.; Strackeljan, J. *A Holistic Approach on the Simulation of Rotary Friction Welding*; Epubli: Magdeburg, Germany, 2015.
24. Kumar Rajak, D.; Pagar, D.D.; Menezes, P.L.; Eyvazian, A. Friction-based welding processes: Friction welding and friction stir welding. *J. Adhes. Sci. Technol.* **2020**, *34*, 2613–2637. [CrossRef]
25. Lu, D.; You, G.; Luo, J.; Ding, Y.; Zeng, S.; Tong, X. Effects of rotational speed on microstructure and mechanical properties of inertia friction-welded 7005–5083 aluminum alloy joints. *J. Mater. Sci.* **2020**, *55*, 12338–12352. [CrossRef]
26. Banerjee, A.; Wylie, A.; Da Silva, L. Near-Net Shape Manufacture of Ultra-High Strength Maraging Steel Using Flow Forming and Inertia Friction Welding: Experimental and Microstructural Characterization. *J. Manuf. Sci. Eng.* **2022**, *145*, 021004. [CrossRef]
27. Beygi, R.; Galvão, I.; Akhavan-Safar, A.; Pouraliakbar, H.; Fallah, V.; da Silva, L.F.M. Effect of Alloying Elements on Intermetallic Formation during Friction Stir Welding of Dissimilar Metals: A Critical Review on Aluminum/Steel. *Metals* **2023**, *13*, 768. [CrossRef]
28. Tolosa, I.; Garciandía, F.; Zubiri, F.; Zapirain, F.; Esnaola, A. Study of mechanical properties of AISI 316 stainless steel processed by "selective laser melting", following different manufacturing strategies. *Int. J. Adv. Manuf. Technol.* **2010**, *51*, 639–647. [CrossRef]
29. Gao, L.L.; Cheng, X.H. Microstructure, phase transformation and wear behavior of Cu–10%Al–4%Fe alloy processed by ECAE. *Mater. Sci. Eng. A* **2008**, *473*, 259–265. [CrossRef]
30. Zoeram, A.S.; Anijdan, S.H.M.; Jafarian, H.R.; Bhattacharjee, T. Welding parameters analysis and microstructural evolution of dissimilar joints in Al/Bronze processed by friction stir welding and their effect on engineering tensile behavior. *Mater. Sci. Eng. A* **2017**, *687*, 288–297. [CrossRef]
31. Murray, J.L. The aluminium-copper system. *Int. Met. Rev.* **1985**, *30*, 211–233. [CrossRef]
32. Impéror-Clerc, M. Three-dimensional periodic complex structures in soft matter: Investigation using scattering methods. *Interface Focus* **2012**, *2*, 589–601. [CrossRef]
33. Xu, X.; Zhao, H.; Hu, Y.; Zong, L.; Qin, J.; Zhang, J.; Shao, J. Effect of hot compression on the microstructure evolution of aluminium bronze alloy. *J. Mater. Res. Technol.* **2022**, *19*, 3760–3776. [CrossRef]
34. Li, L.; Qiao, Y.; Zhang, L.; Ma, A.; Ma, R.; Zheng, Y. Understanding the Corrosion Behavior of Nickel-Aluminum Bronze Induced by Cavitation Corrosion Using Electrochemical Noise: Selective Phase Corrosion and Uniform Corrosion. *Materials* **2023**, *16*, 669. [CrossRef]
35. Ambroziak, A. Carbon diffusion in friction welded joints of refractory metals in a liquid. *Mater. Sci. Eng. A* **2010**, *527*, 6666–6671. [CrossRef]
36. Akbar Akbar, A.A.; Mahdi, B.S.; Aluwi, A.J. Characterization of Diffusion Bonding of Stainless Steel AISI 316 and Pure Titanium sheets Using Copper Interlayer. *IOP Conf. Ser. Mater. Sci. Eng.* **2019**, *518*, 032041. [CrossRef]
37. Gotawala, N.; Shrivastava, A. Investigation of Interfacial Diffusion During Dissimilar Friction Stir Welding. In *Friction Stir Welding and Processing X*; Springer International Publishing: Cham, Switzerland, 2019.
38. Kumar, R.; Balasubramanian, M. Analysis and comparison of diffusion bonded and friction welded Ti-6Al-4V and stainless steel joints with copper as interlayer. *Mater. Today Proc.* **2020**, *21*, 1467–1473. [CrossRef]
39. Xiong, J.-t.; Xie, Q.; Li, J.-l.; Zhang, F.-s.; Huang, W.-d. Diffusion Bonding of Stainless Steel to Copper with Tin Bronze and Gold Interlayers. *J. Mater. Eng. Perform.* **2012**, *21*, 33–37. [CrossRef]
40. Wang, L.-P.; Yang, W.; Ma, Z.-B.; Zhu, J.-H.; Li, Y.-T. First-principles study of chromium diffusion in the ferritic Fe-Cr alloy. *Comput. Mater. Sci.* **2020**, *181*, 109733. [CrossRef]
41. Menzies, I.A.; Mortimer, D. Mechanism of Oxidation of Chromium Diffusion Coatings on Iron. *Nature* **1965**, *208*, 1307–1309. [CrossRef]
42. Kajihara, M.; Yamashina, T. Quantitative analysis for kinetics of reactive diffusion in the Fe–Cr system. *J. Mater. Sci.* **2007**, *42*, 2432–2442. [CrossRef]
43. Sun, H.; Han, Y.; Li, Y. Microstructure and strength of diffusion bonding W alloy/304 stainless steel joint using a Cu interlayer. *Int. J. Refract. Met. Hard Mater.* **2023**, *113*, 106188. [CrossRef]
44. Mitani, Y.; Vargas, R.; Zavala, M. Deformation and diffusion bonding of aluminidecoated steels. *Thin Solid Film.* **1984**, *111*, 37–42. [CrossRef]
45. Rizi, M.S.; Kokabi, A.H. Microstructure evolution and microhardness of friction stir welded cast aluminum bronze. *J. Mater. Process. Technol.* **2014**, *214*, 1524–1529. [CrossRef]
46. Yu, P.; Wu, C.; Shi, L. Analysis and characterization of dynamic recrystallization and grain structure evolution in friction stir welding of aluminum plates. *Acta Mater.* **2021**, *207*, 116692. [CrossRef]
47. Parks, J.M. Recrystallization welding. *Weld. J.* **1953**, *32*, 209s–222s.